

Impact of polarization pulling on optimal spectrometer design for stimulated Brillouin scattering microscopy

Cite as: APL Photon. 9, 100807 (2024); doi: 10.1063/5.0225074
Submitted: 22 June 2024 • Accepted: 23 September 2024 •
Published Online: 23 October 2024



View Online



Export Citation



CrossMark

Jake R. Rosvold,¹ Joseph B. Murray,² Giulia Zanini,¹ Brandon Redding,^{2,a)} and Giuliano Scarcelli^{1,a)}

AFFILIATIONS

¹Fischell Department of Bioengineering, University of Maryland, 8278 Paint Branch Drive, College Park, Maryland 20742, USA

²U.S. Naval Research Laboratory, 4555 Overlook Ave. SW, Washington, District of Columbia 20375, USA

Note: This paper is part of the APL Photonics Special Topic on Brillouin Scattering and Optomechanics.

a) Authors to whom correspondence should be addressed: brandon.f.redding.civ@us.navy.mil and scarc@umd.edu

ABSTRACT

Brillouin spectroscopy has become an important tool for mapping the mechanical properties of biological samples. Recently, stimulated Brillouin scattering (SBS) measurements have emerged in this field as a promising technology for lower noise and higher speed measurements. However, further improvements are fundamentally limited by constraints on the optical power level that can be used in biological samples, which effectively caps the gain and signal-to-noise ratio (SNR) of SBS biological measurements. This limitation is compounded by practical limits on the optical probe power due to detector saturation thresholds. As a result, SBS-based measurements in biological samples have provided minimal improvements (in noise and imaging speed) compared with spontaneous Brillouin microscopy, despite the potential advantages of the nonlinear scattering process. Here, we consider how a SBS spectrometer can circumvent this fundamental trade-off in the low-gain regime by leveraging the polarization dependence of the SBS interaction to effectively filter the signal from the background light via the polarization pulling effect. We present an analytic model of the polarization pulling detection scheme and describe the trade-space unique to Brillouin microscopy applications. We show that an optimized receiver design could provide $>25\times$ improvement in SNR compared to a standard SBS receiver in most typical experimental conditions. We then experimentally validate this model using optical fiber as a simplified test bed. With our experimental parameters, we find that the polarization pulling scheme provides $100\times$ higher SNR than a standard SBS receiver, enabling $100\times$ faster measurements in the low-gain regime. Finally, we discuss the potential for this proposed spectrometer design to benefit low-gain spectroscopy applications such as Brillouin microscopy by enabling pixel dwell times as short as $10\ \mu\text{s}$.

© 2024 Author(s). All article content, except where otherwise noted, is licensed under a Creative Commons Attribution-NonCommercial 4.0 International (CC BY-NC) license (<https://creativecommons.org/licenses/by-nc/4.0/>). <https://doi.org/10.1063/5.0225074>

I. INTRODUCTION

Brillouin spectroscopy has emerged as a powerful tool, specifically in microscopy applications, because it probes the local longitudinal modulus of the sample material.¹ Most Brillouin microscopy methods, which recently have been used in a number of biomechanical studies,^{2–6} rely on the spontaneous Brillouin scattering process. This process measures the characteristic frequency shift of photons, which are inelastically scattered by phonons inherently present in the sample; however, these measurements are limited to, at best, ~ 20 ms spectral acquisition in point-sample configurations^{7,8} and

1 ms in multiplexed scenarios.^{9,10} This fundamental limitation is due to the fact that the scattering efficiency, i.e., the ratio of the power of the scattered and incident light, of the spontaneous process is on the order of 10^{-10} – 10^{-11} in typical biological samples.¹¹ The use of high power to compensate for this weak signal is bounded by the photodamage constraints introduced in the measurement of biological samples, namely thermal damage due to unwanted absorption of the incident light.^{12,13}

An alternative option to spontaneous Brillouin scattering is stimulated Brillouin scattering (SBS), which employs a nonlinear interaction of two light beams with phonons to produce a far

stronger Brillouin scattering signal. To date, *SBS* has been utilized in a wide range of applications; most commonly, *SBS* is used in fiber-optic distributed sensing^{14–16} for temperature or strain measurements but also can be found in optical signal processing¹⁷ and on-chip waveguides.¹⁸ In these scenarios, *SBS* is often orders of magnitude stronger than spontaneous Brillouin scattering due to the long interaction length available in optical fiber and on-chip waveguides. However, in biological samples and for microscopy applications where interaction lengths and optical powers are constrained, the *SBS* gains in signal-to-noise ratio (*SNR*) are significantly diminished because the efficiency of the nonlinear interaction is reduced: with typical parameters used in *SBS* measurements of biological material, the gain can be as low as 10^{-4} – 10^{-5} , meaning that the Brillouin amplified signal is only a small fraction of the detected signal, leading to low *SNR*. As a result, the first demonstrations of *SBS* microscopes using continuous wave lasers required long integration times with spectral acquisitions around 2–20 ms and total power kept to roughly 250 mW.^{19,20} One approach to increasing *SNR* while keeping average power constant is to pulse the interacting beams,^{21,22} thus increasing their peak power, the Brillouin scattering efficiency,²³ and the collected Brillouin amplified signal level; however, demonstrations of this approach have yet to make any speed improvements and have mainly been concerned with reducing the total optical power delivered to the sample. The main reason for this is that the high-speed detectors used in these implementations typically saturate between 1 and 20 mW, which specifically limits the useable peak probe power.

In practical terms, low-gain Brillouin measurements in microscopy settings are taken in a disadvantageous condition where most of the total power is allocated toward the pump, leaving a fraction of the total power budget for the probe. This power imbalance mainly stems from the detection strategy, which measures the *SBS* gain via an amplification of the probe signal and must keep the probe power low enough to avoid saturating the detector—introducing a trade-off between detector sensitivity, bandwidth, and saturation power. To understand this trade-off, consider a typical situation in Brillouin microscopy of biological samples where photodamage concerns limit the total average and peak power to around 200 mW and 2 W, respectively.^{7,19} Under these constraints, the measurement *SNR* is maximized when the available peak power is divided 2:1 between the pump and probe. In reality, detector saturation prevents the use of this optimal power balance, and previous implementations used a ratio closer to 20:1.²¹

In this work, we show how polarization-based detection²⁴ of the *SBS* signal can alleviate detector saturation and improve low-gain *SBS* measurements. Polarization-based detection schemes, also referred to as polarization pulling, have been used for sharp tunable filters,^{25,26} precise frequency comb control,^{27,28} and high-resolution spectroscopy.²⁹ Here, the polarizations of the two *SBS* beams are intentionally misaligned. Consequently, the polarization state of the amplified probe signal is “pulled” toward that of the pump. This effect allows for discrimination, via polarization sensitive detection, between the initial probe light and the “gain” photons, ultimately allowing us to increase the initial probe power without saturating the photodetector, thus increasing the Brillouin amplified signal and the resultant measurement *SNR*. The polarization mismatch, however, comes at the cost of *SBS* efficiency since there is less polarization overlap between pump and probe beams, and approximately half the

gain photons are discarded along with the large probe background. At high gain levels (>~30%), the trade-off between improved signal discrimination and decreased *SBS* efficiency does not lead to a net improvement; however, we show that in the low-gain regime, the benefits of enabling the use of a stronger probe more than compensate for the reduced gain, enabling a >25× improvement in *SNR* and >25× faster spectral acquisition times under practical Brillouin microscopy operating conditions. We experimentally validated this model using an optical fiber platform, which allowed us to tune the Brillouin gain over several orders of magnitude. We show that the polarization pulling scheme enables *SBS* measurements in the low-gain regime (10^{-4}) in just 10 μs with an accuracy of 1/30th of the Brillouin linewidth (equivalent to ~10 MHz for *SBS* interactions in water), an accuracy corresponding to a modulus sensitivity of <0.1%—representing a 100× speed-up compared to the time required for a standard *SBS* measurement to achieve the same accuracy at our experimental parameters.

II. OPERATING PRINCIPLE

In *SBS* spectroscopy, it is desirable to increase the pump and probe power in order to increase the Brillouin gain and achieve higher *SNR* measurements; however, in applications such as microscopy, the sample introduces limits on the average power and peak powers due to photodamage constraints. Pulsing the pump and probe can improve the *SNR* for a fixed average power,^{21,22} but the minimum duty cycle is constrained by the peak power photodamage threshold, limiting the *SNR* improvement. Furthermore, the balance of power between the pump and probe beams should be considered for optimal *SNR*.²¹ When operating in shot-noise conditions, the *SNR* has the following dependence on the pump and probe powers: $SNR \propto P_{pump}^2 P_{probe}$,²⁰ where the *SNR* is defined as the change in the measured probe signal voltage squared due to Brillouin amplification divided by the shot-noise limited uncertainty in the measured probe signal power (also converted to voltage squared). Although *SNR* is maximized for a peak power ratio of $P_{pump} : P_{probe} = 2 : 1$, it is not a trivial matter to use this optimal power balance since the detector saturation prohibits the use of high probe power. Most commercial high-speed detectors saturate between 1 and 20 mW. For example, assuming an average power of 200 mW and a duty cycle of 10%, allocating 33% of the power to the probe would lead to a peak probe power of 667 mW—well beyond the saturation threshold of high-speed photodetectors. Instead, to avoid saturating a detector with a saturation power of 20 mW (as used in Refs. 19–21), only 1% of the power can be allocated to the probe beam, resulting in a 75% reduction in *SNR* compared to the optimal ratio. Ultimately, these constraints on *SBS* measurements result in acquisition times that approach those used in spontaneous Brillouin schemes with little or no improvement.

However, a polarization pulling scheme can help circumvent these limitations by discarding much of the probe power. This approach has the same *SNR* scaling ($SNR \propto P_{pump}^2 P_{probe}$), but the detected power can be greatly reduced, allowing for operation at the optimal 2:1 ratio of the pump to probe powers. While full analytical expressions can be found below, Fig. 1 outlines this trade-space, comparing standard stimulated and spontaneous Brillouin scattering to a stimulated Brillouin scattering approach applying polarization pulling. Here, we assume a spontaneous Brillouin

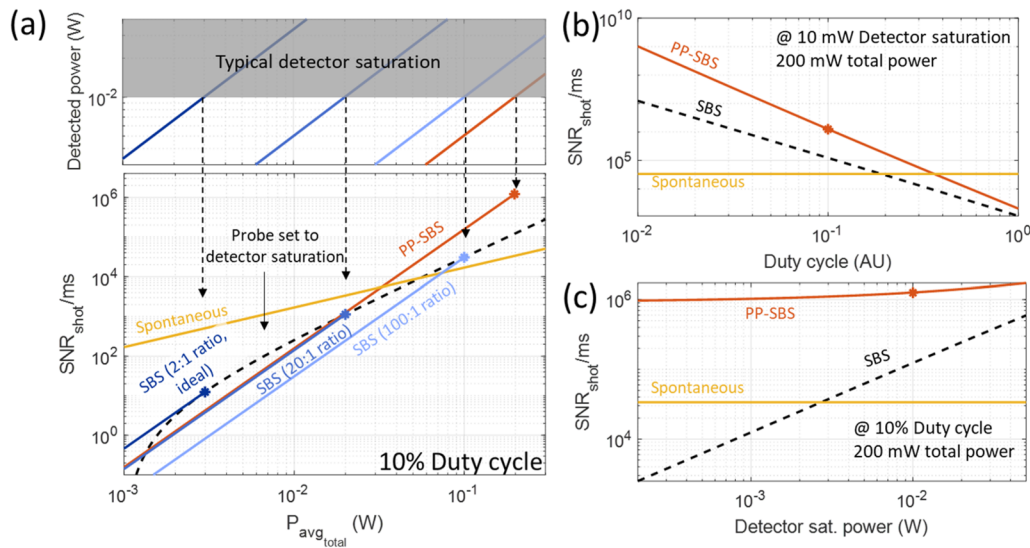


FIG. 1. (a) Demonstration of theoretical shot noise limited SNR (signal power) per ms and detected probe power vs total average power for various implementations of pulsed Brillouin assuming a 10% duty cycle. The yellow line depicts spontaneous scattering (spontaneous), the blue lines show standard SBS with three different ratios of pump-to-probe power, and the orange line depicts a polarization pulling (PP-SBS) approach with a fixed (ideal) 2:1 pump-to-probe power ratio and with polarization sensitive detection rejecting a fixed 98.5% of the probe light. Standard SBS is limited by detector saturation (chosen here to be 10 mW), as shown in the upper plot with dots in the lower plot indicating this point. The dotted line in the lower plot shows the envelope of detector saturation as the pump-to-probe ratio is varied, which sets the probe power to the detector saturation. This limit throttles the standard SBS approach while the polarization pulling scheme can reject much of the original probe power. (b) shows the SNR per ms for SBS, PP-SBS, and spontaneous vs duty cycle for fixed total average power (200 mW) and operating at a fixed detector saturation power (10 mW). Lines depict the optimal pump-to-probe ratio for each approach and at optimal polarization extinction for PP-SBS. (c) Shows the SNR per ms for SBS, PP-SBS, and spontaneous vs detector saturation for fixed total average power (200 mW) and operating at a detector saturation power (10 mW) with a 10% duty cycle. Lines depict the optimal pump-to-probe ratio for each approach and at optimal polarization extinction for PP-SBS.

collection efficiency of 5.4×10^{-11} and a stimulated Brillouin gain coefficient of $1.0 \times 10^{-4} \text{ W}^{-1}$ as typical values for water. We assume a 10% duty cycle unless otherwise noted. Figure 1(a) demonstrates the basic advantage captured by polarization pulling, plotting shot noise limited SNR (signal power divided by noise power) per ms of integration time vs total average power, $\langle P_{probe} \rangle + \langle P_{pump} \rangle$. We assume the polarization sensitive detection rejects 98.5% of the probe power (matching the settings used in the experiments described below), which is optimal at 10 mW detector saturation (see below for detailed analytical expressions). At low powers, the standard SBS using the ideal 2:1 ratio can outperform all other stimulated Brillouin scattering based methods described here, but it is fundamentally throttled by detector saturation (taken here to be 10 mW), such that, at best, it underperforms spontaneous Brillouin measurements by more than a factor of 10. The dashed line represents standard SBS with the power ratio allowed to vary but with the detected probe power fixed at the detector saturation level. Using higher ratios allows for higher detector limited SNR. However, by removing much of the initial probe power, the polarization pulling scheme can operate at much higher powers, using the ideal 2:1 ratio without saturating the detector, resulting in greater SNR (as shown in orange). Figure 1(b) demonstrates how this advantage scales with the duty cycle, assuming a 200 mW average power budget (i.e., $\langle P_{probe} \rangle + \langle P_{pump} \rangle = 200 \text{ mW}$) and with the peak detected power locked at 10 mW. Here, the ratio of pump to probe power is allowed

to vary for optimal SNR and, in the case of polarization pulling, the optimal rejection ratio is used at each point (letting more total light reach the detector as the peak power is reduced while restricting more background probe light as greater peak power is available). The dot depicts the operating point from Fig. 1(a). Polarization pulling significantly outperforms standard SBS at low duty cycles. However, at higher duty cycles the advantage is less pronounced as the polarization extinction ratio must be reduced until the two approaches converge and neither can outperform the spontaneous Brillouin scattering approach. Figure 1(c) shows how SNR varies as the detector saturation limit is adjusted for a 200 mW average power budget and 10% duty cycle with pump-to-probe power ratios and polarization rejection ratios set to optimal values. While the standard approach suffers at lower allowed detector power since it cannot operate at optimal power ratios, the polarization pulling scheme is approximately constant over this range as background light can be continuously reduced to compensate for lower detector saturation. Below, we show how a spectrometer, such as the one designed herein, compares to others in the prior art with respect to microscopy (see Sec. IV below).

Here, we present analytical expressions further describing this trade-space, including other noise sources. Figure 2 shows schematics of the standard SBS measurement and the polarization pulling scheme, as well as the polarization components of the optical fields.

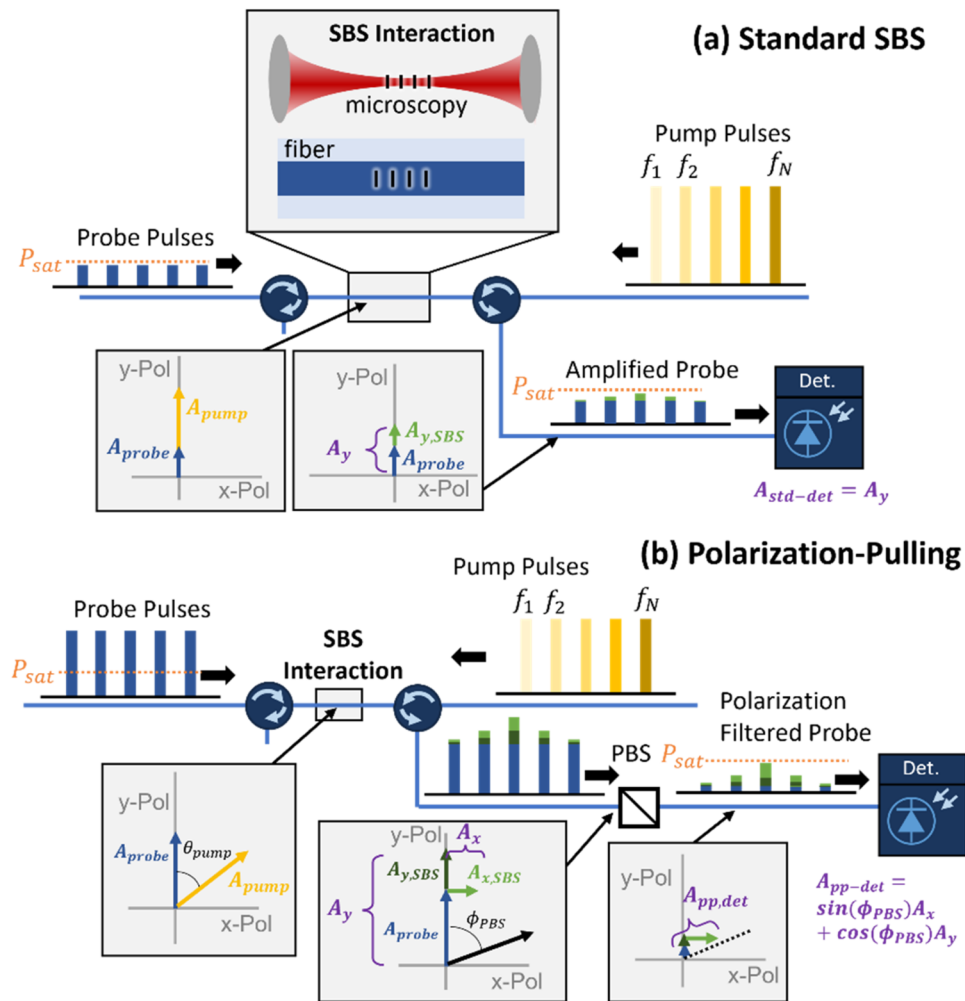


FIG. 2. Schematic depiction of (a) simplified standard SBS and (b) polarization pulling detection schemes (*PBS*: polarizing beam splitter, ϕ_{PBS} : the *PBS* transmission axis with respect to the probe polarization, θ_{pump} : the pump polarization with respect to the probe polarization). Shown in yellow are the pump pulses, in blue are the probe pulses, and in green are the Brillouin amplified probe. Inset field diagrams show the various linear-polarization components of the fields. Note that standard SBS measurements are taken with co-polarized pump and probe fields for maximal gain, whereas in polarization pulling they are intentionally misaligned.

In the standard SBS spectroscopy configuration shown in Fig. 2(a), counter-propagating pump and probe beams have the same polarization and overlap in the “SBS interaction region.” In general, this interaction could take place at the focal point of a microscope, in an optical fiber, a waveguide, or other material of interest. The Brillouin gain spectrum is measured by sweeping the frequency of the pump (or the probe) and recording the amplified probe signal. In Fig. 2, we depict the implementation using pulsed pump and probe beams, although the same basic technique could be applied in CW. However, as discussed earlier, using pulses with a relatively low duty cycle enables better SNR without exceeding the damage thresholds related to average power and peak power. Finally, note that the peak power of the probe pulse train must be low enough to avoid saturating the photodetector (the saturation power is labeled P_{sat} in Fig. 2).

The polarization pulling scheme is shown in Fig. 2(b). In this case, the transmitted probe light passes through a polarizing beam splitter (*PBS*) before reaching the detector. The *PBS* is aligned at an angle ϕ_{PBS} relative to the probe beam in order to reject most of the probe light, enabling the use of a much stronger initial probe beam without saturating the detector. In this scheme, the pump beam polarization is misaligned from the probe by an angle θ_{pump} in order to “pull” the polarization of the amplified probe light toward the polarization of the pump [see the lower left inset in Fig. 2(b)]. The amplified probe light is then preferentially transmitted through the *PBS* for detection. This approach can achieve higher SNR than a standard SBS measurement by enabling the use of a much stronger probe beam without saturating the detector. Below, we use an analytic model of the polarization pulling detection scheme to optimize the system configuration (e.g., the *PBS* angle ϕ_{PBS} and the

pump polarization θ_{pump}) and estimate the potential performance improvement. We then experimentally validate this model using a fiber optic setup, enabling us to compare a standard SBS setup with the polarization pulling scheme over a wide range of Brillouin gain.

To model the SNR of Brillouin measurements obtained using the polarization pulling detection scheme, we need to calculate the detected “signal” level due to SBS amplification. To do this, we first assume that the probe field is aligned in the y polarization and has an initial amplitude, A_{probe} , while the pump beam has amplitude A_{pump} with polarization that is rotated by an angle θ_{pump} with respect to the y -axis [as shown in the lower-left inset in Fig. 2(b)]. After the SBS interaction, the probe field can be decomposed into x and y polarizations with amplitudes A_x and A_y , where $A_x = A_{x,SBS}$ describes the Brillouin amplified field in the x polarization and $A_y = A_{probe} + A_{y,SBS}$ contains both the transmitted probe and the Brillouin amplified field component in the y polarization [see the lower-middle inset in Fig. 2(b)]. We can model the polarization pulling effect due to the misalignment between the pump and probe polarizations by expressing A_x and A_y , which can be derived from the pulling expression in Ref. 30, as

$$A_x = A_{x,SBS} = \sin(\theta_{pump}) \cos(\theta_{pump}) A_{probe} (e^{G_{SBS}/2} - 1), \quad (1a)$$

$$A_y = A_{probe} + A_{y,SBS} = A_{probe} e^{\cos(\theta_{pump}) G_{SBS}/2}, \quad (1b)$$

where G_{SBS} is the Brillouin power gain when the pump and probe polarizations are aligned (i.e., $G_{SBS} \equiv |A_y|^2 / |A_{probe}|^2$ at $\theta_{pump} = 0$). The $\sin(\theta_{pump})$ and $\cos(\theta_{pump})$ terms account for the reduction in Brillouin gain due to misaligning the pump and probe polarization (as $\theta_{pump} \rightarrow 90^\circ$, $A_{x,SBS}$ and $A_{y,SBS} \rightarrow 0$). From these expressions, we see that the polarization pulling effect is most efficient (i.e., A_x is maximized) for $\theta_{pump} = 45^\circ$. Note that these expressions can be applied to both the standard SBS scheme and the polarization pulling scheme by adjusting θ_{pump} .

In a standard SBS measurement with $\theta_{pump} = 0$, the detected probe field amplitude simplifies to $A_{std-det} = A_y = A_{probe} e^{G_{SBS}/2}$ since the $A_x = 0$. We can then calculate the detected “signal” power, $P_{std-signal}$, as the difference between the detected power when the pump is present, $P_{std-SBS}$, and the detected probe power in the absence of SBS, $P_{std-ref}$, as

$$P_{std-signal} = P_{std-SBS} - P_{std-ref}, \quad (2a)$$

$$P_{std-SBS} = A_{std-det}^* A_{std-det}, \quad (2b)$$

$$P_{std-ref} = A_{probe}^* A_{probe}. \quad (2c)$$

Finally, to facilitate comparisons with our experiments, we can convert this detected signal level to measured voltage as $V_{std-signal} = (R_{V/A} \mathcal{R}_{A/W}) P_{std-signal}$, where $R_{V/A}$ is the transimpedance gain in V/A and $\mathcal{R}_{A/W}$ is the detector responsivity in A/W .

In the polarization pulling scheme, the detected probe field after passing through the PBS can be expressed as $A_{pp-det} = \cos(\phi_{PBS}) A_y + \sin(\phi_{PBS}) A_x$. As in the standard SBS case, we can

calculate the detected “signal” power in the polarization pulling configuration, $P_{pp-signal}$, as the difference between the detected power when the pump is present, P_{pp-SBS} , and the detected probe power in the absence of SBS, P_{pp-ref} ,

$$P_{pp-signal} = P_{pp-SBS} - P_{pp-ref}, \quad (3a)$$

$$P_{pp-SBS} = A_{pp-det}^* A_{pp-det}, \quad (3b)$$

$$P_{pp-ref} = \cos^2(\phi_{PBS}) A_{probe}^* A_{probe}. \quad (3c)$$

Under typical operating conditions where $G_{SBS} \ll 1$ (typically $\sim 10^{-5}$), $\theta_{pump} = 45^\circ$, and ϕ_{PBS} is adjusted to provide reasonable extinction such that $G_{SBS} \ll \sin^2(\phi_{PBS}) \ll 1$ (typically $10^{-1} - 10^{-3}$), Eqs. (1)–(3) can be simplified to

$$P_{pp-signal} \cong \sin(\theta_{pump}) \cos(\theta_{pump}) P_{probe} (G_{SBS}/2). \quad (3d)$$

Again, the measured signal level in the polarization pulling case can be converted to voltage as $V_{pp-signal} = (R_{V/A} \mathcal{R}_{A/W}) P_{pp-signal}$.

Using Eqs. (1)–(3), we can calculate the measured “signal” level for the standard and polarization pulling schemes as a function of Brillouin gain as well as the orientation of the pump polarization, θ_{pump} , and the PBS, ϕ_{PBS} . In order to estimate the SNR and the measurement uncertainty (or the acquisition time required to reach a desired uncertainty), we also need to estimate the measurement noise. We can describe the measurement noise in terms of the RMS voltage uncertainty, σ_V , during a measurement of an amplified probe pulse of duration τ . In the ideal case, σ_V will be dominated by shot-noise, σ_{V-shot} , although experimentally, noise from the photodetector, σ_{V-det} , or the analog to digital converter (ADC), σ_{V-ADC} , could also be significant, especially as $\phi_{PBS} \rightarrow 90^\circ$ and the power reaching the detector is reduced. Other possible noise sources such as amplified spontaneous emission (ASE) and relative intensity noise (RIN) could be significant in some implementations but are not accounted for here. Our model analyzes a best-case system, and with our choice of a low RIN seed laser and minimal amplification stages, RIN and ASE noise were insignificant. In our model, we estimated the contribution from each of these noise sources using the following expressions:

$$\sigma_{V-shot} = R_{V/A} \sqrt{2q P_{det} \mathcal{R}_{A/W} / \tau}, \quad (4a)$$

$$\sigma_{V-ADC} = \sigma_{V-ADC,0} / \sqrt{f_{ADC} \tau}, \quad (4b)$$

$$\sigma_{V-det} = R_{V/A} \mathcal{R}_{A/W} P_{NEP} \sqrt{1/\tau}, \quad (4c)$$

where q is the charge of an electron, P_{det} is the total optical power reaching the detector (e.g., $P_{det} = P_{pp-SBS} + P_{pp-ref}$), $\sigma_{V-ADC,0}$ is the RMS voltage uncertainty per sample of the ADC at a sample rate f_{ADC} , and P_{NEP} is the noise equivalent power of the photodetector. The total voltage uncertainty over a pulse length τ was given by summing each of these noise sources in quadrature. We can then calculate the SNR using the expressions for the signal level in voltage listed earlier as

$$\text{SNR}_\tau = \left[\frac{V_{\text{signal}}}{\sigma_V} \right]^2. \quad (5)$$

In the case of shot limited noise and under the typical operating assumptions described earlier, $\text{SNR}_{\tau\text{-shot}} \cong [\cos(\theta_{\text{pump}})P_{\text{probe}}(G_{\text{SBS}}/2)\mathcal{R}_{A/W}]^2/(2q/\tau) \propto P_{\text{pump}}^2P_{\text{probe}}$. Therefore, polarization pulling has the same SNR scaling with pump and probe peak powers as the standard method. Finally, we use this SNR estimate to calculate the uncertainty in the measured Brillouin frequency as an amplitude spectral density (ASD_f) in units of $\text{Hz}/\sqrt{\text{Hz}}$, assuming quadratic fitting over the FWHM of the measured peak, as³¹

$$\text{ASD}_f = \sqrt{\frac{3}{4}} \left[\frac{1}{\sqrt{\text{SNR}_\tau}} \right] \frac{\Gamma_B}{\sqrt{\text{PRF}/2}} \sqrt{\Delta f_{\text{scan}}/\Gamma_B}, \quad (6)$$

where Γ_B is the Brillouin linewidth, PRF is the pulse repetition frequency, and Δf_{scan} is the bandwidth the pump is swept over to obtain a measurement of the gain spectrum [see Appendix for the full derivation of Eq. (6)]. The $\sqrt{\Delta f_{\text{scan}}/\Gamma_B}$ term accounts for the trade-off between dynamic range and measurement uncertainty

since the measurements outside the Brillouin gain spectrum do not provide significant additional information. The leading $\sqrt{3}/4$ fraction assumes a quadratic fit of the peak and would negligibly change if Lorentzian fitting was used instead. Note that the frequency ASD is to a good approximation, independent of the number of frequency steps taken across the scan bandwidth, as long as at least three frequency steps were taken within the Brillouin linewidth.³¹ Of course, the number of frequency steps will still impact the minimum time required to complete a frequency scan and obtain a measurement, but this can be quite short (e.g., 10 μs in our experiments described below). The ASD can then be used to estimate the frequency uncertainty in a given measurement time, T , as $\sigma_f = \text{ASD}_f/\sqrt{2T}$ or the time required to obtain a measurement with a desired precision, σ_f , as $T = (1/2)(\text{ASD}_f/\sigma_f)^2$ (assuming white noise). Consequently, using ASD instead of the commonly used frequency precision or frequency uncertainty in Brillouin microscopy provides a convenient metric that is independent of the time required to obtain a frequency scan.

Finally, we used these expressions to calculate the signal level and ASD obtained in the standard and polarization pulling schemes as a function of θ_{pump} and ϕ_{PBS} , as shown in Fig. 3. The Brillouin

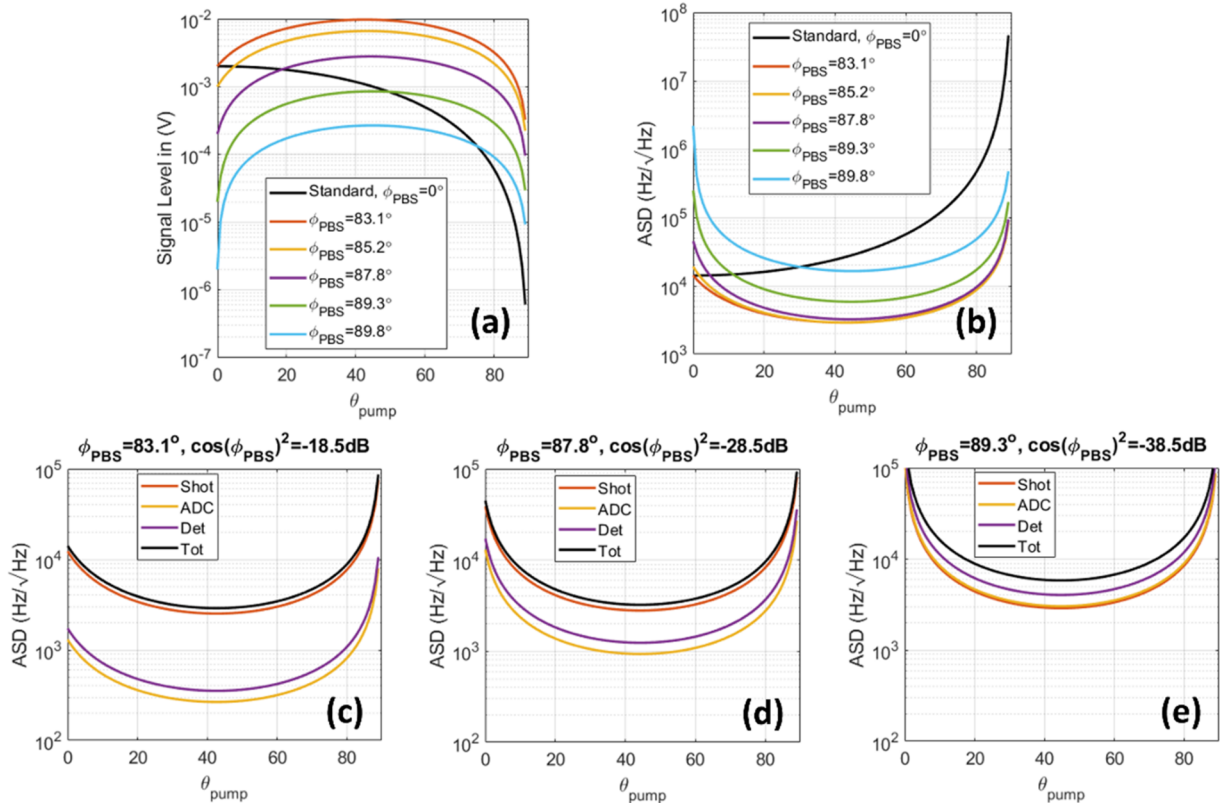


FIG. 3. Demonstration of noise model performance metrics. (a) The Brillouin amplified signal level and (b) ASD as a function of the angle between the pump and the probe beams. The colored lines indicate various extinction levels in the polarization pulling configuration. Notice at modest extinction, the ability of polarization pulling to achieve higher signal levels and, therefore, lower ASD when the pump angle is roughly 45° . The black line represents the standard SBS signal level which is maximized when the pump and probe are co-polarized. (c)–(e) ASD due to various noise sources as a function of the angle between the pump and the probe beams across multiple extinction levels.

gain was set to $G_{SBS} = 2 \times 10^{-4}$. In these simulations, we selected detection parameters to match our experiments. Specifically, we assumed a photodetector with $\mathcal{R}_{A/W} = 1A/W$, $R_{V/A} = 700 V/W$, $P_{NEP} = 10^{-12} W/\sqrt{Hz}$, and $P_{sat} = 1.4 mW$ and an ADC with $\sigma_{V-ADC,0} = 0.5 mV$ and $f_{ADC} = 1GS/s$. The pump and probe beams were both pulsed at a 10% duty cycle with a pulse duration $\tau = 100 ns$ and $PRF = 1 MHz$. The scan bandwidth was set to $\Delta f_{scan} = 2\Gamma_b = 60 MHz$ (using the Brillouin linewidth for standard optical fiber).

In the standard SBS simulations, we set the peak probe power to 1.4 mW, as required, to avoid saturating the photodetector. In the polarization pulling simulation, the peak probe power was set to 48.5 mW to avoid saturating the detector at the lowest ϕ_{PBS} considered. As shown in Fig. 3(a), the signal level in the standard case, shown in black, decreases monotonically with θ_{pump} (as expected, there is no advantage to misaligning the pump and probe polarization in the standard case). However, in the polarization pulling case, the signal level is maximized for $\theta_{pump} = 45^\circ$ for each ϕ_{PBS} setting. We also found that the actual measured signal level in the polarization pulling case can be higher than in the standard case for $\phi_{PBS} < \sim 87.8^\circ$. Of course, increasing the signal level by reducing ϕ_{PBS} also results in higher background probe power hitting the detector, which will increase the shot noise. To evaluate this trade-off, we can consider the ASD shown in Fig. 3(b). In the standard case, the ASD increases with θ_{pump} , as expected. However, in the polarization pulling case, we find that the ASD is minimized for $\theta_{pump} = 45^\circ$ and can actually be a factor of ~ 10 lower than the ASD obtained in the standard case because of the higher, useable probe power. We also find that the minimum ASD is relatively constant for $\phi_{PBS} \sim 87.8^\circ$. In this regime, the measurement is shot-noise limited, and adjusting the probe extinction at the PBS does not change the overall measurement precision. As $\phi_{PBS} \rightarrow 90^\circ$, the signal and background probe light are both significantly reduced, and the detector and ADC noise begin to dominate [see Figs. 3(c)–3(e) for the impact of different noise sources at varying ϕ_{PBS}], resulting in the higher ASD noise shown in Fig. 3(b) for $\phi_{PBS} > \sim 89.3^\circ$.

To summarize, these simulations indicate that the polarization pulling scheme is most efficient for $\theta_{pump} = 45^\circ$. Somewhat surprisingly, high extinction at the PBS is not required and can actually

make the measurement more sensitive to detector and ADC noise. Note that setting ϕ_{PBS} in the range of 83.1° to 87.8° corresponds to 18.4–28.3 dB of extinction, which is easily obtained with most commercial polarizers and polarizing beam splitters. Crucially, this analysis also confirms that polarization pulling has the potential for significantly higher SNR than standard SBS measurements in applications where the power allocated to the probe beam is limited by the saturation threshold of the photodetector. As a result, polarization pulling could significantly accelerate Brillouin microscopy measurements since an improvement in ASD of $10\times$ corresponds to a $100\times$ decrease in acquisition time for the same measurement precision.

III. EXPERIMENTAL DEMONSTRATION

In order to validate our model and confirm that polarization pulling does in fact result in higher SNR measurements, we conducted experiments using a fiber optic platform where the Brillouin gain can be easily varied over several orders of magnitude. As shown in Fig. 4, both the pump and probe arms were seeded with the same narrowband laser (kHz linewidth, RIO Orion) operating at ITU Channel 32 (193.2 THz). Using the same seed laser for the pump and probe reduces the sensitivity to laser frequency noise, particularly in spectroscopy applications where the pump and probe arms can be path matched. Along the upper path, an electro-optic modulator (EOM) was used to generate the frequency shifted pump pulses with a duration of 100 ns and a repetition period of 1 μs (10% duty cycle). The pulse duration and duty cycle were chosen to be common and relevant values for microscopy applications. The EOM was driven in carrier suppressed mode, and the frequency of the 100 ns bursts increased in 10 steps from 10.81 to 10.87 GHz, covering a 60 MHz band corresponding to twice the Brillouin linewidth in the fiber ($\Gamma_B \sim 30 MHz$). The system completed a frequency scan every 10 μs . Using a high-speed AWG (Tektronix AWG70001B) to drive the EOM in this way provides a versatile platform with easily adjustable pulse duration, duty cycle, frequency step size, and scan range.

After the EOM, light was directed to a tunable bandpass filter (Santec OTF-980), which selected the upper sideband. An erbium

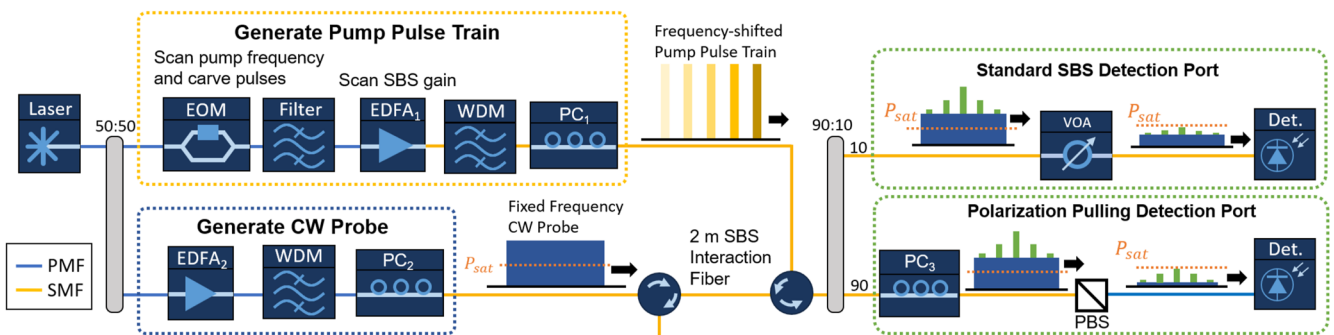


FIG. 4. Diagram of the experimental setup used in this work. The upper path was used to generate the pulsed pump train. The lower path generates the CW probe beam. When operating with the standard SBS port, the polarization controls in the pump and probe paths (PC₁ and PC₂) are used to co-polarize the two beams and maximize the Brillouin gain in the 2 m interaction fiber. To use the polarization pulling port, PC₃ is adjusted to avoid saturating the detector, and PC₁ is adjusted to maximize the signal level, setting the pump polarization to $\sim 45^\circ$ relative to the probe. Note the solid blue lines indicate polarization maintaining fiber (PMF), whereas solid orange lines indicate single mode fiber (SMF).

doped fiber amplifier (EDFA₁) was then used to control the power of the pump pulses in order to adjust the *SBS* gain. A 100 GHz-wide wavelength division multiplexing (WDM) filter was positioned after the EDFA to suppress amplified spontaneous emission. The pump pulses were then directed through a polarization controller (PC₁) before coupling into the *SBS* interaction region through a fiber circulator. The *SBS* interaction region consisted of 2 m of single mode optical fiber (SMF-28 Ultra) held straight at uniform tension to ensure a consistent Brillouin frequency and to minimize polarization rotation within the 2 m segment of fiber (note that polarization dispersion in SMF-28 Ultra results in ~200 nm in path mismatch between polarization states in this case). In the probe path, the seed laser was amplified by EDFA₂, directed through another WDM filter, and passed through a polarization controller (PC₂) before entering the interaction fiber through a circulator. The Brillouin amplified probe light was then split between a standard *SBS* detection port (consisting of a variable attenuator and a detector) and the polarization pulling detection port (consisting of a fiber-coupled polarizing beam splitter and a detector). In both cases, we used 125 MHz photodetectors with a saturation power of ~1.4 mW (Teratec, TTI-525), and the detected signal was digitized using a 1 GS/s ADC. A 100 ns moving average was applied to suppress digitizer noise.

Note that in these experiments, we used a CW probe for simplicity rather than the pulsed probe shown in Fig. 2. Since the photodamage was not a concern using the fiber sample, this allowed us to demonstrate the principle of polarization pulling without requiring an additional modulator. For our experiments, the probe power in the interaction fiber was ~50 mW. In the future, pulsing the probe at the same 10% duty cycle as the pump would reduce the average power in the *SBS* interaction region (to minimize photodamage) without impacting the measurement SNR.

We first confirmed that the polarization state was relatively constant in the straight section of optical fiber by evaluating our

ability to modulate the Brillouin gain as we adjusted the pump and probe paddles. If the polarization varied along the fiber, then the pump and probe beams would always overlap in polarization at some positions along the fiber, preventing us from fully suppressing the Brillouin amplification.³² Indeed, in our initial tests using a coiled fiber, polarization rotation in the interaction fiber prevented us from significantly suppressing the Brillouin gain. However, using a straight fiber at uniform tension, we were able to fully modulate the Brillouin gain from maximum down to ~-20 dB compared to the maximum gain (matching our measurement accuracy), confirming that the polarization state was uniform along the fiber.

We then performed a series of measurements using the standard *SBS* port to quantify the baseline measurement uncertainty over a wide range of Brillouin gain values. A variable optical attenuator (VOA) was used to set the detected probe power just below the saturation level of the photodetector. In practice, rather than using a VOA, a lower initial power probe should be used to minimize power in the *SBS* interaction region. However, positioning the VOA in the *SBS* detection port path, rather than, e.g., reducing the gain on EDFA₂, does not impact the measurement SNR on the standard port and allows us to more easily switch between the two detection ports. We then aligned the polarization of the pump and probe beams using PC₁ and PC₂ to maximize the measured gain on the standard port detector.

At each pump power setting, we recorded the transmitted probe beam for 10 ms, providing 1000 measurements of the Brillouin gain spectrum (each measurement is completed during a 10 μs frequency scan). We applied a Lorentzian fit to each 10 μs measurement to estimate the Brillouin frequency and calculated the ASD.³³ We also extracted the gain and measured the signal level [using the definition in Eq. (2)] for comparison with our model. Note that at low gain ($G_{SBS} < 10^{-3}$), the standard port does not have sufficient SNR to provide a reliable measurement of the Brillouin frequency shift using a single 10 μs frequency scan. To obtain a more reliable measurement

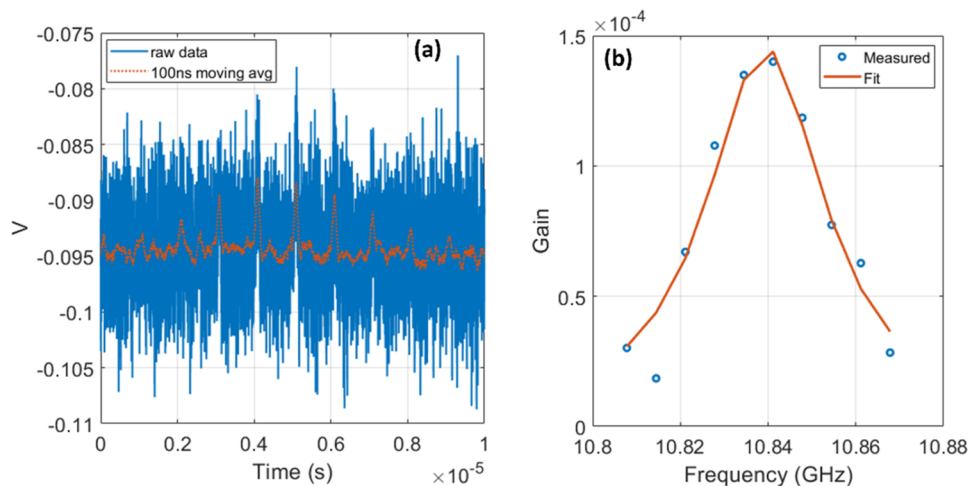


FIG. 5. (a) The raw data recorded in the polarization pulling port in 10 μs representing a single frequency scan across 60 MHz in 10 discrete steps using 100 ns pump pulses at a 10% duty cycle. Note that the AC coupled detector had a voltage offset of -0.094 V. (b) The gain spectrum measured on the polarization pulling port normalized to G_{SBS} measured using the standard *SBS* port at the same pump power.

at these gain values, we first averaged 10 sequential frequency scans before performing the Lorentzian fit and updated the ASD calculation to account for a 10× increase in the effective time required to complete a frequency scan.

We then performed a series of measurements over the same range of pump powers using the polarization pulling setup. In this case, we first adjusted PC_3 so that the probe power transmitted through the PBS and reaching the polarization pulling detector was just below the saturation level. Based on the measured probe power of ~77 mW exiting the interaction fiber, this corresponded to a $\phi_{PBS} \sim 83^\circ$ and attenuation at the PBS of ~19 dB. We then adjusted the pump polarization using PC_1 to maximize the signal level due to Brillouin amplification observed on the polarization pulling detector. Based on the model presented earlier, this corresponds to $\theta_{pump} \sim 45^\circ$. We then recorded a series of measurements at the same pump power settings used on the standard port. For each pump power, we again recorded the transmitted probe for 10 ms and applied a Lorentzian fit to the gain spectrum obtained from each 10 μs frequency scan. The data obtained with an AC coupled detector during a typical 10 μs scan is shown in Fig. 5(a) at a pump power

that corresponded to $G_{SBS} \sim 1.4 \times 10^{-4}$ on the standard port. We first applied a 100 ns moving average to the raw data acquired at 1 GS/s to match the 100 ns pump pulse duration and suppress the digitizer noise present in the raw data. We then selected the “signal” due to Brillouin amplification based on the definition in Eq. (3) as the difference between the measured voltage at the center of each pump pulse and the average background voltage level. The resulting gain spectrum was then fit with a Lorentzian, as shown in Fig. 5(b). This procedure was repeated for 1000 frequency scans at 9 pump powers, corresponding to G_{SBS} in the range of 10^{-4} to 10^{-2} . Unlike the standard SBS port, the measurements on the polarization pulling port had sufficient SNR to reliably extract the Brillouin frequency in a 10 μs frequency scan down to the lowest G_{SBS} measured of $\sim 9 \times 10^{-5}$. For example, the measurement uncertainty obtained in a 10 μs scan at $G_{SBS} \sim 1.4 \times 10^{-4}$ was ~1 MHz, corresponding to ~1/30th of the Brillouin linewidth in optical fiber.

We then compared the measurements obtained on the standard and polarization pulling ports with our model. The measured signal levels obtained as a function of G_{SBS} are shown in Fig. 6(a). This measurement shows excellent agreement with our model over

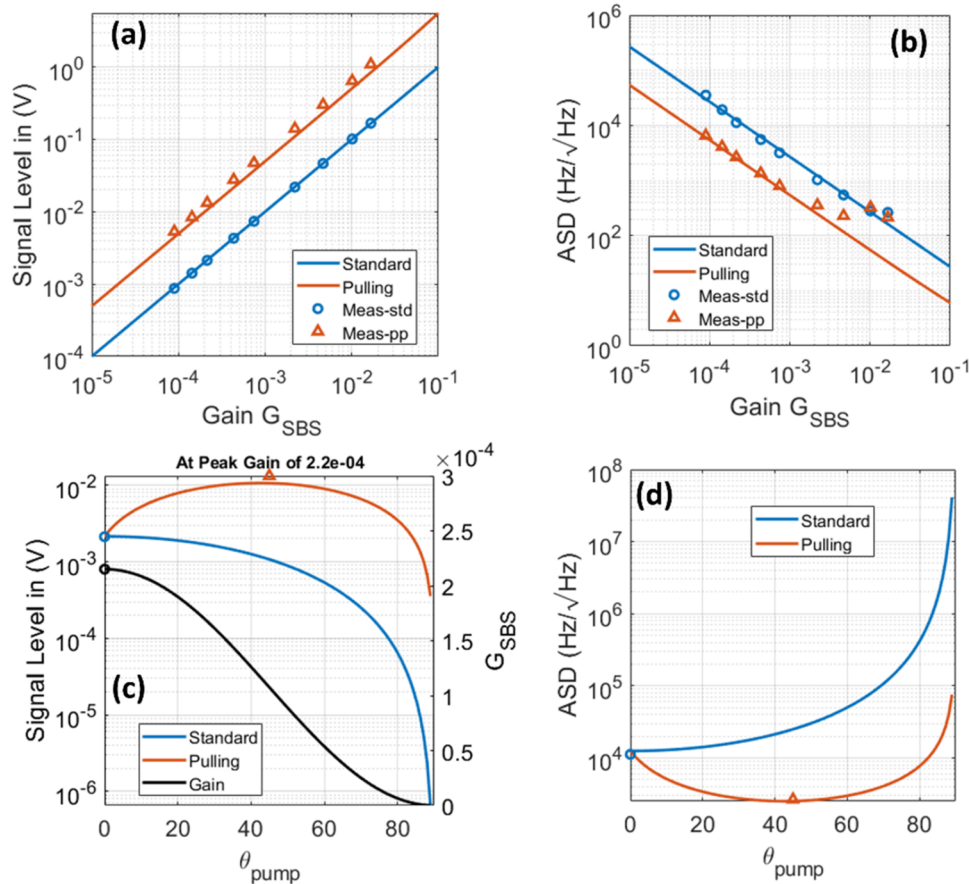


FIG. 6. Demonstration of experimental results compared with our noise model. (a) The Brillouin amplified signal level and (b) ASD as a function of gain. At high pump powers, back-reflected pump light increases the measured ASD. (c) The Brillouin amplified signal level in the respective optimal conditions compared to the model. Gain, in black, corresponds to the right Y-axis title and is marked at the standard SBS peak gain. (d) Measured ASD in the respective optimal conditions compared to the model with a $\phi_{PBS} \sim 83^\circ$.

the full range of G_{SBS} and confirms that the polarization pulling scheme is able to obtain a higher measured signal level, in agreement with the prediction shown in Fig. 3(a). We then compared the measured frequency uncertainty ASD over the same range of G_{SBS} , as shown in Fig. 6(b). We found a good agreement with the model for gain below $\sim 10^{-3}$. At higher gain, reflected pump light due to Rayleigh backscattering and/or imperfections in the fiber circulators began to degrade the measurement obtained on the polarization pulling port. This is not present in the standard port because the VOA attenuates both the probe and pump light equally; however, the polarization pulling port is more sensitive to this kind of background signal since the detection leverages a PBS that is specifically aligned to suppress the probe light while transmitting a higher fraction of the backscattered pump light. In the future, a narrowband spectral filter could be used to reject pump light before it reaches the detector.^{19,20,22} Nonetheless, this measurement confirmed that the polarization pulling detection scheme can provide a $\sim 10\times$ reduction in ASD in low-gain measurements where the probe power is limited by the detector saturation threshold.

Finally, we compared the measured signal level and ASD as a function of θ_{pump} at a gain of $G_{SBS} = 2 \times 10^{-4}$, as shown in Figs. 6(c) and 6(d). Again, the signal and ASD agree well with our model and indicate that we are operating near the optimal conditions for a polarization pulling measurement.

IV. DISCUSSION

The polarization pulling detection scheme presented in this work is particularly well-suited for Brillouin microscopy measurements in the biological regime. Brillouin microscopy has traditionally relied on spontaneous Brillouin scattering; however, in recent years, SBS has been proposed due to its potential for increased efficiency and reduced measurement times. In practice, SBS has provided only a modest speed-up since the damage thresholds in biological materials limit the pump and probe power, restricting SBS measurements to the low-gain regime (10^{-5} to 10^{-4}). Recent work has shown that pulsing the pump and probe lasers could partially alleviate this concern^{21,22} by maintaining a fixed average power while increasing the peak power. However, pulsing the probe can result in peak powers that are well beyond the saturation threshold of commercially available photodetectors. This makes it difficult to use the optimal $\sim 2:1$ distribution of pump to probe power. The polarization pulling scheme presented here was designed to address this restriction by discarding most of the background probe light before it reaches the detector.

In this work, we presented an analytic model showing that this approach has the potential for a $>25\times$ improvement in SNR compared to standard SBS measurements in typical Brillouin microscope conditions, assuming commercially available detectors with saturation power in the 1–20 mW range. We then experimentally validated this model using a fiber optic platform that allowed us to easily vary the Brillouin gain over several orders of magnitude. Although the fiber platform has significant differences from a biological sample, we can normalize these distinctions to compare the polarization pulling measurements presented in this work to recent SBS measurements in biological microscopy applications. First, the Brillouin linewidth in optical fiber of ~ 30 MHz is $\sim 10\times$ narrower than in most biological samples, as well as water,

which has a linewidth of ~ 300 MHz and is commonly used to benchmark biological Brillouin microscopy systems. As shown in Eq. (6), the measurement uncertainty is proportional to the Brillouin linewidth. As a result, we cannot directly compare the measured frequency uncertainty in fiber and water but need to be normalized by the Brillouin linewidth. Second, most Brillouin microscopes report the acquisition time required to obtain biologically relevant accuracy, typically $\sim \Gamma/30$.^{2,34,35} We therefore converted the measured ASD shown in Fig. 6(b) to the time required to obtain a measurement with a normalized uncertainty of $\Gamma/30$ as $t_{\Gamma/30} = \frac{1}{2} (ASD_f / \sigma_{\Gamma/30})^2$, where the target uncertainty $\sigma_{\Gamma/30} = 1$ MHz for optical fiber. Third, as shown in Eq. (6), the uncertainty also depends on the frequency scan bandwidth. Optimal biological measurements use a scan bandwidth of $\sim 2\Gamma$,²¹ which matches the normalized scan bandwidth used in this work. Finally, since we are comparing measurements with different materials, interaction lengths, and pump powers, we can compare $t_{\Gamma/30}$ as a function of Brillouin gain, which dictates the measured signal level. As discussed earlier, for a fixed average power, using a pulsed pump and probe beams will increase the measured gain, SNR , and reduce the required measurement time for a fixed precision.²¹ To compare measurements performed at different duty cycles, we normalize by the *duty-cycle* $\times G_{SBS}$ product. This normalization implies that a sample that provides a CW gain of 10^{-5} at the maximum allowed average power of 200 mW could be probed at a 10% duty cycle to obtain a peak gain of 10^{-4} . The $t_{\Gamma/30}$ at a given *duty-cycle* $\times G_{SBS}$ product then allows us to compare the acquisition time (pixel dwell time) required to obtain an accuracy of $\Gamma/30$ for a fixed material, interaction length, and average power.

We applied this normalization to both the standard SBS and polarization pulling measurements reported earlier in Fig. 6. As shown in Fig. 7, the standard SBS measurements obtained in fiber agree relatively well with a series of recent experimental measurements recorded in water over a range of *duty-cycle* $\times G_{SBS}$ products. In contrast, the polarization pulling measurements shown in Fig. 7 show a $\sim 100\times$ shorter acquisition time compared to the standard SBS measurements. For example, at a *duty-cycle* $\times G_{SBS}$ product of 1.4×10^{-5} , the polarization pulling scheme achieves the target frequency uncertainty of $\Gamma/30$ in just $10 \mu s$ (i.e., a single frequency scan in the experiments presented here), compared to Refs. 19 and 20, which required ~ 3 ms to achieve the same uncertainty using standard SBS detection. This would represent a dramatic improvement in image acquisition time in a Brillouin microscopy application. In this respect, scanning over twice the Brillouin linewidth is optimal for the performance of Brillouin microscopy systems where the material is known; however, it is common to use a larger scan bandwidth of 2–4 GHz when the sample is unknown. In this case, the time required to reach a target accuracy would increase in proportion to the scan bandwidth [see Eq. (6)]. For example, increasing the scan bandwidth from $\sim 2\Gamma$ to $\sim 10\Gamma$ (to provide a 3 GHz scan bandwidth) would increase acquisition by a factor of 5. A demonstration of this technology in microscopy could be achieved by integrating the pump and probe beams in a counterpropagating microscope and using polarization-control waveplates in place of the fiber-based polarization control paddles used in this work. In addition, it would be prudent to change the operating wavelength to the visible or near infrared regime (e.g., ~ 780 nm is often used in Brillouin microscopy) where water absorption is less significant.

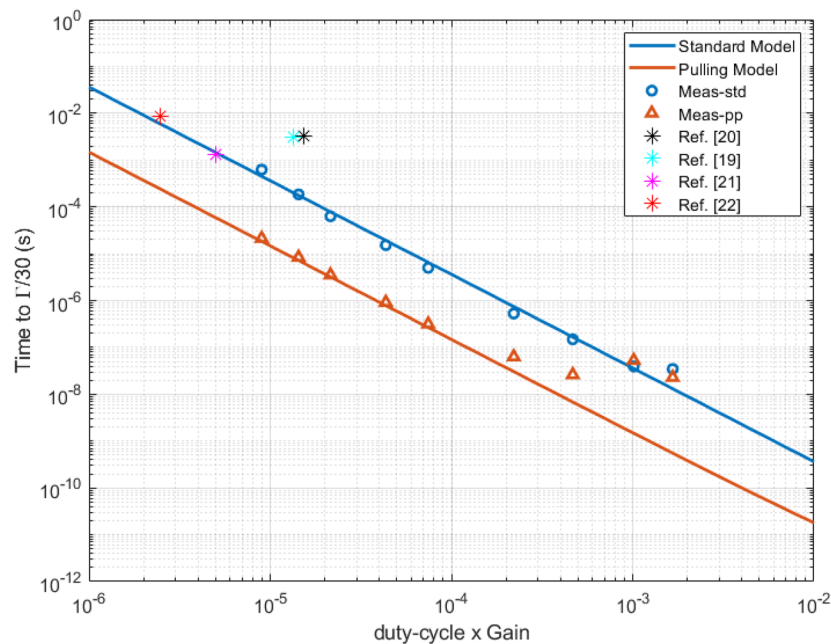


FIG. 7. Measured standard and polarization pulling SBS results compared to our noise model and a few recent SBS microscopy publications, as denoted in the legend, on normalized axes describing the measurement time needed to achieve a frequency uncertainty of $\Gamma/30$ vs the product of duty-cycle and gain. Of note, Refs. 19 and 20 both operate with a CW pump and probe, whereas Refs. 21 and 22 use pulsed pump and probe beams. Polarization pulling offers a significant speed-up compared to current Brillouin spectrometers.

V. CONCLUSION

In this work, we introduced a polarization pulling based SBS detection scheme. This technique separates the Brillouin amplified light from the background probe light, enabling the use of a strong probe beam without exceeding the detector saturation threshold. We developed an analytic model of the polarization pulling detection process, which indicated that this approach could provide a significant increase in SNR compared to a standard SBS detection scheme using standard photodetectors with saturation thresholds in the 1–20 mW range. We experimentally validated this model using a fiber optic platform, confirming that the polarization pulling technique can provide a $>25\times$ improvement in SNR. Finally, we analyzed how this detection scheme could impact Brillouin microscopy measurements in the low-gain regime, indicating the potential for a $>25\times$ increase in imaging speed.

SUPPLEMENTARY MATERIAL

A derivation of Eq. (6) is provided in the [supplementary material](#).

ACKNOWLEDGMENTS

The work was supported by the U.S. Naval Research Laboratory and the National Institutes of Health under Grant No. R21CA258008.

AUTHOR DECLARATIONS

Conflict of Interest

The authors have no conflicts to disclose.

Author Contributions

J.R.R. and J.B.M. contributed equally to this work.

Jake R. Rosvold: Data curation (equal); Formal analysis (equal); Investigation (equal); Methodology (equal); Validation (equal); Writing – original draft (equal); Writing – review & editing (equal). **Joseph B. Murray:** Conceptualization (equal); Formal analysis (equal); Methodology (equal); Validation (equal); Writing – original draft (equal); Writing – review & editing (equal). **Giulia Zanini:** Formal analysis (supporting); Validation (supporting); Writing – review & editing (supporting). **Brandon Redding:** Conceptualization (equal); Funding acquisition (equal); Supervision (equal); Writing – original draft (equal); Writing – review & editing (equal). **Giuliano Scarcelli:** Conceptualization (equal); Funding acquisition (equal); Supervision (equal); Writing – original draft (equal); Writing – review & editing (equal).

DATA AVAILABILITY

The data that support the findings of this study are available from the corresponding authors upon reasonable request.

REFERENCES

- ¹J. Randall and J. M. Vaughan, "The measurement and interpretation of Brillouin scattering in the lens of the eye," *Proc. R. Soc. Lond. B.* **214**(1197), 449–470 (1982).
- ²G. Scarcelli, S. Besner, R. Pineda, P. Kalout, and S. H. Yun, "In vivo biomechanical mapping of normal and keratoconus corneas," *JAMA Ophthalmol.* **133**(4), 480 (2015).
- ³G. Scarcelli, W. J. Polacheck, H. T. Nia, K. Patel, A. J. Grodzinsky, R. D. Kamm, and S. H. Yun, "Noncontact three-dimensional mapping of intracellular hydromechanical properties by Brillouin microscopy," *Nat. Methods* **12**(12), 1132–1134 (2015).
- ⁴E. O. Wisniewski, P. Mistriotis, K. Bera, R. A. Law, J. Zhang, M. Nikolic, M. Weiger, M. Parlani, S. Tuntithavornwat, A. Afthinos, R. Zhao, D. Wirtz, P. Kalab, G. Scarcelli, P. Friedl, and K. Konstantopoulos, "Dorsoventral polarity directs cell responses to migration track geometries," *Sci. Adv.* **6**(31), eaba6505 (2020).
- ⁵J. Zhang, F. Alisafaei, M. Nikolić, X. A. Nou, H. Kim, V. B. Shenoy, and G. Scarcelli, "Nuclear mechanics within intact cells is regulated by cytoskeletal network and internal nanostructures," *Small* **16**(18), 1907688 (2020).
- ⁶R. Schlüsler, S. Möllmert, S. Abuhattum, G. Cojoc, P. Müller, K. Kim, C. Möckel, C. Zimmermann, J. Czarske, and J. Guck, "Mechanical mapping of spinal cord growth and repair in living zebrafish larvae by Brillouin imaging," *Biophys. J.* **115**(5), 911–923 (2018).
- ⁷M. Nikolić and G. Scarcelli, "Long-term Brillouin imaging of live cells with reduced absorption-mediated damage at 660 nm wavelength," *Biomed. Opt. Express* **10**(4), 1567 (2019).
- ⁸J. Zhang and G. Scarcelli, "Mapping mechanical properties of biological materials via an add-on Brillouin module to confocal microscopes," *Nat. Protoc.* **16**(2), 1251–1275 (2021).
- ⁹C. Bevilacqua, J. M. Gomez, U.-M. Fiuza, C. J. Chan, L. Wang, S. Hambura, M. Eguren, J. Ellenberg, A. Diz-Muñoz, M. Leptin, and R. Prevedel, "High-resolution line-scan Brillouin microscopy for live imaging of mechanical properties during embryo development," *Nat. Methods* **20**(5), 755–760 (2023).
- ¹⁰J. Zhang, M. Nikolic, K. Tanner, and G. Scarcelli, "Rapid biomechanical imaging at low irradiation level via dual line-scanning Brillouin microscopy," *Nat. Methods* **20**(5), 677–681 (2023).
- ¹¹P. Shao, A. M. Eltony, T. G. Seiler, B. Tavakol, R. Pineda, T. Koller, T. Seiler, and S.-H. Yun, "Spatially-resolved Brillouin spectroscopy reveals biomechanical abnormalities in mild to advanced keratoconus in vivo," *Sci. Rep.* **9**(1), 7467 (2019).
- ¹²S. Wäldchen, J. Lehmann, T. Klein, S. Van De Linde, and M. Sauer, "Light-induced cell damage in live-cell super-resolution microscopy," *Sci. Rep.* **5**(1), 15348 (2015).
- ¹³P. P. Laissue, R. A. Alghamdi, P. Tomancak, E. G. Reynaud, and H. Shroff, "Assessing phototoxicity in live fluorescence imaging," *Nat. Methods* **14**(7), 657–661 (2017).
- ¹⁴T. Horiguchi, K. Shimizu, T. Kurashima, M. Tateda, and Y. Koyamada, "Development of a distributed sensing technique using Brillouin scattering," *J. Lightwave Technol.* **13**(7), 1296–1302 (1995).
- ¹⁵D. M. Chow, Z. Yang, M. A. Soto, and L. Thévenaz, "Distributed forward Brillouin sensor based on local light phase recovery," *Nat. Commun.* **9**(1), 2990 (2018).
- ¹⁶J. B. Murray and B. Redding, "Suppressing non-local effects due to Doppler frequency shifts in dynamic Brillouin fiber sensors," *Opt. Express* **28**(8), 10760 (2020).
- ¹⁷M. Santagiustina, S. Chin, N. Primerov, L. Ursini, and L. Thévenaz, "All-optical signal processing using dynamic Brillouin gratings," *Sci. Rep.* **3**(1), 1594 (2013).
- ¹⁸D. Marpaung, B. Morrison, M. Pagani, R. Pant, D.-Y. Choi, B. Luther-Davies, S. J. Madden, and B. J. Eggleton, "Low-power, chip-based stimulated Brillouin scattering microwave photonic filter with ultrahigh selectivity," *Optica* **2**(2), 76 (2015).
- ¹⁹I. Remer, R. Shaashoua, N. Shemesh, A. Ben-Zvi, and A. Bilenca, "High-sensitivity and high-specificity biomechanical imaging by stimulated Brillouin scattering microscopy," *Nat. Methods* **17**(9), 913–916 (2020).
- ²⁰G. Zanini and G. Scarcelli, "Localization-assisted stimulated Brillouin scattering spectroscopy," *APL Photonics* **7**(5), 056101 (2022).
- ²¹D. M. Chow and S.-H. Yun, "Pulsed stimulated Brillouin microscopy," *Opt. Express* **31**(12), 19818 (2023).
- ²²F. Yang, C. Bevilacqua, S. Hambura, A. Neves, A. Gopalan, K. Watanabe, M. Govendir, M. Bernabeu, J. Ellenberg, A. Diz-Muñoz, S. Köhler, G. Rapti, M. Jechlinger, and R. Prevedel, "Pulsed stimulated Brillouin microscopy enables high-sensitivity mechanical imaging of live and fragile biological specimens," *Nat. Methods* **20**(12), 1971 (2023).
- ²³R. W. Boyd, K. Rzaewski, and P. Narum, "Noise initiation of stimulated Brillouin scattering," *Phys. Rev. A* **42**(9), 5514–5521 (1990).
- ²⁴A. Zadok, E. Zilka, A. Eyal, L. Thévenaz, and M. Tur, "Vector analysis of stimulated Brillouin scattering amplification in standard single-mode fibers," *Opt. Express* **16**(26), 21692 (2008).
- ²⁵A. Wise, M. Tur, and A. Zadok, "Sharp tunable optical filters based on the polarization attributes of stimulated Brillouin scattering," *Opt. Express* **19**(22), 21945 (2011).
- ²⁶Y. Stern, K. Zhong, T. Schneider, R. Zhang, Y. Ben-Ezra, M. Tur, and A. Zadok, "Tunable sharp and highly selective microwave-photonic band-pass filters based on stimulated Brillouin scattering," *Photonics Res.* **2**(4), B18 (2014).
- ²⁷B. Redding, J. D. McKinney, R. T. Schermer, and J. B. Murray, "High-resolution wide-band optical frequency comb control using stimulated Brillouin scattering," *Opt. Express* **30**(12), 22097 (2022).
- ²⁸S. Preußler, N. Wenzel, R.-P. Braun, N. Owschimikow, C. Vogel, A. Deninger, A. Zadok, U. Woggon, and T. Schneider, "Generation of ultra-narrow, stable and tunable millimeter- and terahertz- waves with very low phase noise," *Opt. Express* **21**(20), 23950 (2013).
- ²⁹S. Preussler and T. Schneider, "Attometer resolution spectral analysis based on polarization pulling assisted Brillouin scattering merged with heterodyne detection," *Opt. Express* **23**(20), 26879 (2015).
- ³⁰D.-P. Zhou, Y. Dong, L. Chen, and X. Bao, "Four-wave mixing analysis of Brillouin dynamic grating in a polarization-maintaining fiber: Theory and experiment," *Opt. Express* **19**(21), 20785 (2011).
- ³¹M. A. Soto and L. Thévenaz, "Modeling and evaluating the performance of Brillouin distributed optical fiber sensors," *Opt. Express* **21**(25), 31347 (2013).
- ³²M. O. Van Deventer and A. J. Boot, "Polarization properties of stimulated Brillouin scattering in single-mode fibers," *J. Lightwave Technol.* **12**(4), 585–590 (1994).
- ³³H. Schmid, How to use the FFT and Matlab's pwelch function for signal and noise simulations and measurements, <http://www.schmid-werren.ch/hanspeter/publications/2012fftnoise.pdf>.
- ³⁴G. Scarcelli, R. Pineda, and S. H. Yun, "Brillouin optical microscopy for corneal biomechanics," *Invest. Ophthalmol. Vis. Sci.* **53**(1), 185 (2012).
- ³⁵G. Scarcelli, P. Kim, and S. H. Yun, "In vivo measurement of age-related stiffening in the crystalline lens by Brillouin optical microscopy," *Biophys. J.* **101**(6), 1539–1545 (2011).